Phonon density of states and oxygen-isotope effect in $Ba_{1-x}K_xBiO_3$

C.-K. Loong
Intense Pulsed Neutron Source, Argonne National Laboratory, Argonne, Illinois 60439-4814

P. Vashishta, R. K. Kalia, Wei Jin, and M. H. Degani*
Concurrent Computing Laboratory for Materials Simulations and Department of Physics and Astronomy, Louisiana State University, Baton Rouge, Louisiana 70803-4001

D. G. Hinks, D. L. Price, J. D. Jorgensen, B. Dabrowski, A. W. Mitchell, D. R. Richards, and Y. Zheng
Materials Science Division, Argonne National Laboratory, Argonne, Illinois 60439-4843
(Received 12 September 1991)

The phonon densities of states (DOS) of insulating $BaBiO_3$ and superconducting $Ba_{0.6}K_{0.4}BiO_3$ and the variation of the phonon spectrum of the superconducting compound upon oxygen-isotope (^{16}O, ^{18}O) substitution are determined by inelastic neutron scattering (INS) and molecular-dynamics (MD) simulations. The MD simulations are carried out with an effective interaction potential which includes steric effects, Coulomb interactions, and the charge-dipole interactions due to the electronic polarizability of O^{2-}. The MD results are in good agreement with the INS experiments and electron-tunneling measurements. Partial DOS of Ba, K, Bi, and O in $BaBiO_3$ and $Ba_{0.6}K_{0.4}BiO_3$ are also determined from MD simulations. In the superconducting material, the phonon spectrum softens and is comprised of broad bands around 15, 30, and 60 meV. The partial DOS reveal that phonons above 20 meV are due to oxygen vibrations, whereas phonons below 20 meV are due to Ba, K, and Bi. The reference oxygen-isotope-effect exponent, $\alpha_{O,r}=-\partial \ln\langle\omega\rangle/\partial \ln M_O$, of $Ba_{0.6}K_{0.4}BiO_3$ is determined to be $\alpha_{O,r}=0.42\pm0.05$ from the mass (M_O) variation of the first moment of the phonon DOS, $^{16}O\langle\omega\rangle$ and $^{18}O\langle\omega\rangle$. This value is close to the oxygen-isotope-effect exponent, α_O, determined from the variation of T_c (0.41 ± 0.03 by Hinks *et al.* and 0.35 ± 0.05 by Kondoh *et al.*), indicating that $Ba_{0.6}K_{0.4}BiO_3$ is a weak- to moderate-coupling BCS-like superconductor and that the high T_c (~ 30 K) results from large electron-phonon matrix elements involving high-energy oxygen-related phonons.

I. INTRODUCTION

The physical mechanism responsible for high-temperature superconductivity in the oxide materials has been a focus of intensive research in condensed matter physics since 1986.[1] In general, there are two kinds of oxide superconductors: one containing copper and the other without any transition-metal elements.[1,2] The common structural features of all of the copper-oxide superconductors is the presence of one or more CuO_2 planes.[1,2] Each copper atom in such a plane is strongly bonded to oxygen in a nearly square-planar arrangement.[2] The crucial CuO_2 planes can occur singly or in groups. Among materials which do not contain copper, $Ba_{1-x}K_xBiO_3$ exhibits the highest superconducting transition temperature ($T_c=30$ K for $x\approx0.4$).[3-8] It is of interest to compare the physical properties of this system with those of the high-T_c cuprate superconductors. The superconducting phase of $Ba_{1-x}K_xBiO_3$ ($0.37<x<0.5$) forms a cubic perovskite crystal structure[9] which shows none of the planar structures observed in the other high-T_c compounds (see Fig. 1). $Ba_{1-x}K_xBiO_3$ is nonmagnetic[4,10] while the other related high-T_c copper-oxide materials, in their parent nonsuperconducting phases, display antiferromagnetism.[1] Hall-effect measurements[11] in $Ba_{1-x}K_xBiO_3$ indicate that the carriers are electrons, whereas in cuprates, with the exception of $R_{2-x}Ce_xCuO_4$ ($R=$Pr,Nd), the carriers are holes.[1] There are also important features common to all high-T_c oxide superconductors.[12] First, the normal-state charge carrier density is low (compared with the conventional metallic systems, such as the $A15$ compounds[13]), reflecting the ionic character of the parent materials. Second, superconductivity often occurs near the phase boundary of an insulator-metal transition.[9] As certain critical dopant concentration is reached, metallic behavior (and superconductivity) disappears and a change of the crystal structure often occurs.[9] To achieve a microscopic understanding of the nature of superconductivity in these cubic oxide materials, it is important to understand the role of phonons and their interactions with conduction electrons, charge and/or spin fluctuations in both the insulating and metallic (superconducting) phases.

The importance of electron-phonon interactions in $Ba_{1-x}K_xBiO_3$ has been revealed by measurements of the oxygen-isotope effect in T_c. Batlogg *et al.*[5] measured the oxygen-isotope effect by determining the shift in T_c be-

tween a 100% ^{16}O sample and a 65% ^{18}O exchanged sample of $Ba_{0.6}K_{0.4}BiO_3$. They obtained an exponent $\alpha_O=0.22\pm0.03$ in the $T_c\sim M_O^{-\alpha_O}$ relation, where M_O is the mass of the oxygen isotope.[5] Hinks *et al.*[14] also measured the oxygen-isotope effect for a 100% ^{16}O sample and a 96% ^{18}O exchange sample of $Ba_{0.625}K_{0.375}BiO_3$ and obtained $\alpha_O=0.41\pm0.03$. Kondoh *et al.*[11] synthesized three samples, $Ba_{0.7}K_{0.3}Bi^{16}O_3$, $Ba_{0.7}K_{0.3}Bi^{18}O_3$, and $Ba_{0.7}K_{0.3}Bi[(^{16}O)_{1.5}(^{18}O)_{1.5}]$ and measured T_c from the temperature dependence of Meissner diamagnetism. They obtained $\alpha_O=0.35\pm0.05$. In general, these values are larger than the oxygen-isotope-effect exponents (~0.1) in the cuprate superconductors,[15] although large values of α_O have recently been reported[16] in $La_{2-x}Sr_xCuO_4$ and $(Y_{1-x}Pr_x)Ba_2Cu_3O_7$ for some values of x.

Tunneling spectroscopy also provides valuable information on the strength of electron-phonon coupling. The electron-tunneling measurements on polycrystalline $Ba_{1-x}K_xBiO_3$ by Zasadzinski *et al.*[17] reveal well-resolved structures in the second derivative of bias voltage with respect to tunneling current in the energy range 30–60 meV. Recent tunneling experiments on thin films of $Ba_{0.6}K_{0.4}BiO_3$ by Sato *et al.*[18] yield the ratio $2\Delta(0)/k_BT_c=3.7\pm0.5$, where $\Delta(0)$ is the superconducting energy gap at zero temperature, which is in agreement with the optically derived gap ratio by Schlesinger *et al.*[19] Using point-contact junctions, Huang *et al.*[20] have recently carried out electron-tunneling experiments on $Ba_{1-x}K_xBiO_3$ and $Nd_{2-x}Ce_xCuO_{4-y}$. They observed clear evidence of phonon images in tunneling conductance up to 60 meV. The quality of their experimental data is sufficiently good that it has been possible to obtain the Eliashberg functions $\alpha^2F(\omega)$ for $Ba_{0.625}K_{0.375}BiO_3$. Even though the quality of their tunneling data deteriorates at high energies, they have clearly established[20] that high-energy phonons are involved in superconductivity, that the electron-phonon coupling constant $\lambda\sim1$, and that $2\Delta(0)/k_BT_c=3.8\pm0.1$.

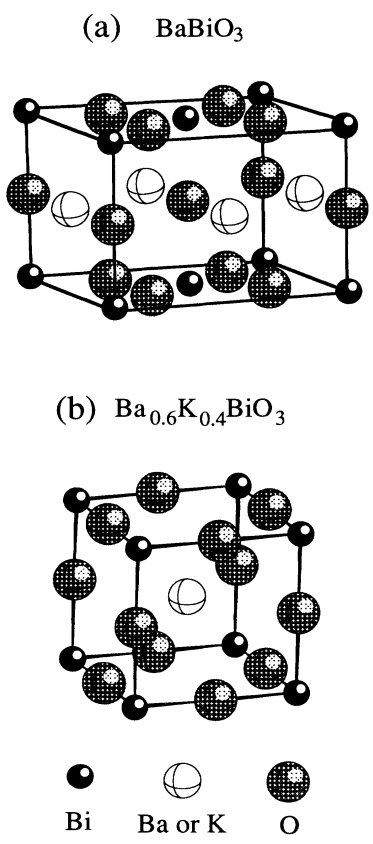

FIG. 1. Crystal structures of (a) orthorhombic $BaBiO_3$ and (b) cubic $Ba_{0.6}K_{0.4}BiO_3$.

In a detailed neutron power diffraction study, Pei *et al.*[9] find that, in this material, superconductivity occurs at the phase boundary of an insulator-metal transition in the vicinity of $x\approx0.35$. As the potassium doping is reduced, superconductivity disappears when the cubic structure distorts through a tilting of the BiO_6 octahedra, resulting in an orthorhombic supercell structure. When the dopant concentration is further decreased to $x<0.1$, an orthorhombic-to-monoclinic transformation occurs which may involve symmetric oxygen breathing-mode distortions.[9] Strong coupling of atomic displacements and charge fluctuations of the Bi ions has been proposed to explain the insulator-metal transition and the semiconducting behavior in the orthorhombic phase.[21] In this picture rapid charge fluctuations between the two inequivalent Bi sites due to strong intra-atomic repulsion coupled to oxygen atomic displacements lead to the formation of charge-density waves (CDW) and the opening of a pseudogap at the Fermi surface.[21] The experimental situation on the existence of charge-density waves in $Ba_{1-x}K_xBiO_3$ has not been resolved to date. Both x-ray- and neutron power diffraction studies show no evidence of long-range CDW ordering.[9] Electron diffraction,[22] on the other hand, reveals an incommensurate modulation along a "pseudocubic" [110] direction. However, whether this modulation is the manifestation of CDW or an artifact induced by the electron beam remains unclear. In any case, both theory and experiment point to the importance of phonons in the $Ba_{1-x}K_xBiO_3$ material.[23,24]

The aforementioned experimental evidence suggests the importance of electron-phonon interactions in $Ba_{1-x}K_xBiO_3$. An understanding of the nature of superconductivity and lattice instabilities, however, requires the knowledge of the phonon excitation spectra in this material. Therefore, we have initiated a systematic investigation of the phonon spectra of this system by a combined study by inelastic-neutron-scattering (INS) and molecular-dynamics (MD) simulations. In this paper we report the determination of the phonon densities of states of superconducting $Ba_{1-x}K_xBi(^{16}O)_3$ and $Ba_{1-x}K_xBi(^{18}O)_3$ ($x=0.4$), and of insulating $Ba_{1-x}K_xBi(^{16}O)_3$ ($x=0$ and 0.2). In the superconducting material, we find significant softening of the oxygen phonon modes around 30 and 60 meV. The variation of the phonon spectrum in superconducting $Ba_{0.6}K_{0.4}BiO_3$ upon oxygen isotope (^{16}O,^{18}O) substitution is determined by INS. The reference oxygen-isotope-effect exponent, α_{Or}, is determined from the mass variation of the first frequency moment of the phonon density of states (DOS),

$\langle\omega\rangle \sim M_O^{-\alpha_{Or}}$. For a monatomic system, the mass variation of the phonon DOS is characterized by the relation $\langle\omega\rangle \sim M^{-1/2}$, consequently, $\alpha_{Or}=0.5$. For a multicomponent system, however, α_{Or} is, in general, not equal to 0.5. In order to characterize the nature of superconductivity within the framework of BCS-Eliashberg theory,[25,26] we investigate the correlation between the isotope shifts in the phonon DOS and in T_c of $Ba_{0.6}K_{0.4}Bi(^{16}O)_3$ and $Ba_{0.6}K_{0.4}Bi(^{18}O)_3$. By combining the INS results with the MD simulations, we obtain a value of $\alpha_{Or}=0.42\pm0.05$ for $Ba_{0.6}K_{0.4}BiO_3$. This is close to the isotope effect exponent in T_c; the measurements of Kondoh *et al.*'s[11] yield $\alpha_O=0.35\pm0.05$ and those of Hinks *et al.*[14] find $\alpha_O=0.41\pm0.03$. These experiments indicate that a measure of strong-coupling effects, $\delta\alpha_O=\alpha_{Or}-\alpha_O$, is small.[27] The results of our study indicate that $Ba_{1-x}K_xBiO_3$ is a weak- to moderate-coupling BCS superconductor. The high superconducting transition temperature (30 K) results from large electron-phonon matrix elements involving high-energy oxygen modes. Brief accounts of the main results have been presented in previous papers.[28,19]

In Sec. II of this paper, we discuss experimental details of neutron-scattering measurements and sample preparation. Section III presents the generalized phonon DOS from neutron experiments. The molecular-dynamics simulations are discussed in Sec. IV. In Sec. V, INS results are compared with the MD simulations. The connection between INS and MD results with the oxygen-isotope effect and tunneling data is also discussed. In Sec. VI, we compare the results for the reference isotope effect exponent with the isotope effect in T_c. Implications of these results on the nature of superconductivity in this material are also discussed.

II. EXPERIMENTAL DETAILS

A. Neutron scattering

Inelastic-neutron-scattering experiments on polycrystalline samples were performed using the high-resolution and low-resolution medium-energy chopper spectrometer (HRMECS and LRMECS) at the Intense Pulsed Neutron Source (IPNS) of Argonne National Laboratory. Pulsed spallation neutron sources have large fluxes of epithermal neutrons and are particularly well suited for investigation of high-energy ($20<E<80$ meV) phonons. The time-of-flight neutron spectrometers at IPNS are equipped with wide-angle multidetector banks that allow measurements of inelastic scattering over a wide range of momentum and energy transfer, see Fig. 2.

The dynamic structure factor at constant scattering angle ϕ is obtained from the observed intensity in terms of the double-differential cross section $d^2\sigma/d\Omega\,dE'$,

$$S(\phi,E)=\frac{4\pi}{\bar{\sigma}}\sqrt{E_0/E'}\frac{d^2\sigma}{d\Omega\,dE'}\ , \tag{1}$$

where E_0 and E' are the incident and scattered neutron energies, respectively, $\bar{\sigma}$ is the total bound atoms scattering cross section per scattering unit, and $E=E_0-E'$ is the energy transfer. The momentum transfer $\hbar Q$ is obtained from the relation

$$\hbar Q=2m_n(E_0+E'-2\sqrt{E_0E'}\cos\phi)^{1/2}\ , \tag{2}$$

where m_n is the neutron mass. Using E_0 of 120 meV with $3°<\phi<120°$, Q extends to values (1–12 Å^{-1}) much larger than the dimension of the first Brillouin zone of the crystal reciprocal lattice. Since a polycrystalline sample is used, the average over all crystallographic orientations becomes an intrinsic part of the experiment. Under these conditions, it can be shown[30] that the phonon density of states of the system, apart from weighting factors σ_i/M_i (where σ_i and M_i are the neutron cross section and the mass, respectively, for the ith atomic species), can be reliably obtained under the incoherent approximation.

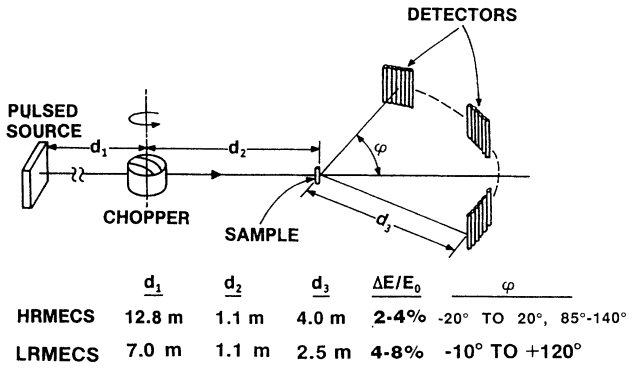

	d_1	d_2	d_3	$\Delta E/E_0$	φ
HRMECS	12.8 m	1.1 m	4.0 m	2-4%	-20° TO 20°, 85°-140°
LRMECS	7.0 m	1.1 m	2.5 m	4-8%	-10° TO +120°

FIG. 2. Schematic diagram of the IPNS chopper spectrometers.

The energy resolution ΔE in full width at half maximum of HRMECS (LRMECS) varies from approximately 4% (8%) of the incident energy in the elastic region to ~2% (4%) near the end of the neutron-energy-loss spectrum. The better resolution of the HRMECS is essential to differentiate fine structure in the phonon DOS of samples containing different K concentrations or of different O isotopes. Polycrystalline samples of $BaBi(^{16}O)_3$, $Ba_{0.8}K_{0.2}Bi(^{16}O)_3$, $Ba_{0.6}K_{0.4}Bi(^{16}O)_3$, and $Ba_{0.6}K_{0.4}Bi(^{18}O)_3$, each about 100 g, were used in the measurements. The samples, contained in aluminum planar cells, were mounted at a 45° angle to the incident neutron beam. Such a geometry decreases the neutron traverse length in the sample to <5 mm for all detector angles thereby reducing multiple-scattering effects. Multiple scattering was estimated to be less than 5% of the total measured intensity. To reduce multiple-phonon excitations, the sample were cooled to 15 K for the experiments. Background scattering was subtracted from the data by using empty-container runs. Measurements of elastic incoherent scattering from a vanadium standard provided detector calibration and intensity normalization.

The generalized energy distribution function, $G(Q,E)$, in the neutron-energy-loss spectrum is defined by[31]

$$G(Q,E)=\frac{2M}{\hbar^2}\frac{n(E)+1}{Q^2}Ee^{2W(Q)}S(Q,E)\ , \tag{3}$$

where M is a mean sample mass, $2W(Q)$ is the Debye-Waller exponent, $n(E)$ is the Bose-Einstein distribution function, and $S(Q,E)$ is the measured dynamic structure factor. For a multicomponent system, the neutron-weighted phonon DOS, in the incoherent approximation, is obtained by the average of $G(Q,E)$ over a wide range of Q, i.e.,

$$G(E)=e^{2\overline{W}}\sum_i \frac{c_i\sigma_i}{M_i}\langle(\hat{\mathbf{Q}}\cdot\hat{\mathbf{e}}_i)^2 e^{-2W_i}\rangle F_i(E)$$
$$\approx \sum_i \frac{c_i\sigma_i}{M_i}F_i(E)\ , \quad (4)$$

where c_i, M_i, σ_i, and $F_i(E)$ are the concentration, mass, neutron-scattering cross section, and partial-phonon DOS for the ith atomic species. In Eq. (4), $\hat{\mathbf{Q}}$ and $\hat{\mathbf{e}}$ are the unit neutron wave vector and phonon polarization vector, respectively, and $\langle\cdots\rangle$ represents the average over all Q directions. The directional Q dependence and the Debye-Waller factors can be neglected in the present case because the measurements were made at low temperatures on polycrystalline material over a range of Q much larger than the dimension of the Brillouin zone. The neutron-weighted phonon DOS includes contributions from multiphonon and multiple-scattering events. The multiphonon component was calculated and subtracted off from the data by a method using an incoherent monatomic harmonic approximation.[31,32] It is difficult to calculate the multiple-scattering component without a realistic scattering kernel. However, since the multiple scattering is expected to produce a smooth background, it is corrected by subtracting off a neutron-flight time-independent background about 5% of the total intensity. In general, correction for multiphonon and multiple scattering produced only minor effects on the results of the phonon DOS.

B. Materials preparation

Polycrystalline samples of $BaBi(^{16}O)_3$, $Ba_{0.8}K_{0.2}Bi(^{16}O)_3$, and $Ba_{0.6}K_{0.4}Bi(^{16}O)_3$ were prepared by a melt-process technique. Metal oxides (K_2O, BaO, and Bi_2O_3) at the stoichiometric metal-ion compositions were melted in a Pt crucible and then quenched onto a copper plate. This reactive material was rapidly transferred into a fused silica furnace tube under a flowing Ar atmosphere. The material was heated to 700 °C at a rate of 2 °C/min under flowing Ar, followed by rapid cooling to room temperature (RT). The furnace tube environment was changed to pure, flowing O_2 and the sample was heated to 400 °C and 2 °C/min, held for 1 h, and cooled to RT at 2 °C/min.

The ^{18}O isotopically exchanged sample $Ba_{0.6}K_{0.4}Bi(^{18}O)_3$ could not be prepared by direct gas exchange. Because of the large sample size (nominally 100 g) with its large oxygen content relative to that of the exchange-gas volume, the exchange of ^{16}O with the surrounding $^{18}O_2$ gas is negligible. The exchange was accomplished using a two-step process.[6] Essentially, the material is first reduced to an effective Bi^{3+} oxidation state (i.e., $Ba_{0.6}K_{0.4}BiO_{2.3}$), all the exchange then occurs through oxygen-vacancy filling. The material was contained in a gold foil within a fused silica furnace tube and heated to 710 °C at 20 °C/min in flowing nitrogen. It was held at this temperature for 20 h and then rapidly cooled to RT. The system was then sealed and evacuated, followed by pressurizing to approximately 150 Torr with $^{18}O_2$ gas (97.5% enriched) from a bulb immersed in liquid nitrogen containing $^{18}O_2$ liquid. The oxygen vacancies were filled by heating the sample to 400 °C, holding for 2 h, followed by cooling to room temperature; both cooling and heating rates were 1 °C/min. This two-step process was repeated seven times. The expected fraction of ^{18}O after seven cycles was calculated to be 82% (ignoring any gas exchange). Experimentally, using thermogravimetric analysis, the exchange fraction was found to be (74±2)%.

The x-ray-diffraction patterns of the $Ba_{0.6}K_{0.4}Bi(^{16}O)_3$ and $Ba_{0.6}K_{0.4}Bi(^{18}O)_3$ samples showed sharp diffraction peaks indicating no detrimental effects on the $Ba_{0.6}K_{0.4}Bi(^{18}O)_3$ sample due to the ^{18}O exchange procedure. The superconducting transition, monitored by ac susceptibility measurements, remained sharp for both samples. In general, both samples are equivalent with respect to purity and structural perfection.

III. GENERALIZED PHONON DENSITY OF STATES FROM INELASTIC NEUTRON SCATTERING

The dynamic structure factor $S(Q,E)$ for insulating $BaBiO_3$ and superconducting $Ba_{0.6}K_{0.4}BiO_3$ obtained from LRMECS measurements with a neutron incident energy of 120 meV is shown in Fig. 3. The neutron-weighted phonon DOE, $G(E)$, derived from these measurements have been published as Figs. 2(a) and 4(a) in a previous paper.[28] In order to better resolve the structure in the DOS of $BaBiO_3$ and $Ba_{0.6}K_{0.4}BiO_3$, we have repeated the measurements using the HRMECS. To understand the role of K disorder, measurements were also made on insulating orthorhombic $Ba_{0.8}K_{0.2}BiO_3$ using the HRMECS. Figure 4 shows the measured neutron-weighted generalized phonon DOS, $G(E)$, of superconducting $Ba_{0.6}K_{0.4}BiO_3$, and insulating $Ba_{0.8}K_{0.2}BiO_3$ and $BaBiO_3$. For $BaBiO_3$, the phonon spectrum shows prominent peaks at 17, 26, 32, 43, 50, 62, and 70 meV. In addition, there is an indication of two shoulders at 10 and 75 meV. The DOS of insulating $Ba_{0.8}K_{0.2}BiO_3$ shows similar features but the peaks are broadened significantly due to K disordering. In the case of the superconducting $Ba_{0.6}K_{0.4}BiO_3$, Fig. 4 shows a qualitatively different phonon DOS than those of the insulating compounds. First, the overall spectrum above 20 meV shifts toward lower energies, resulting in a cutoff of the DOS at about 70 meV, whereas in $Ba_{0.8}K_{0.2}BiO_3$ and $BaBiO_3$, the DOS extends beyond 70 meV with substantial weights. Second, the phonon population in the 40–50-meV region is markedly reduced. Consequently, the DOS of $Ba_{0.6}K_{0.4}BiO_3$ comprises of three broad bands centered around 15, 30, and 60 meV.

We have also measured the phonon DOS of ^{16}O and ^{18}O samples of $Ba_{0.6}K_{0.4}BiO_3$ in order to determine the variation of the phonon spectrum of the superconductor

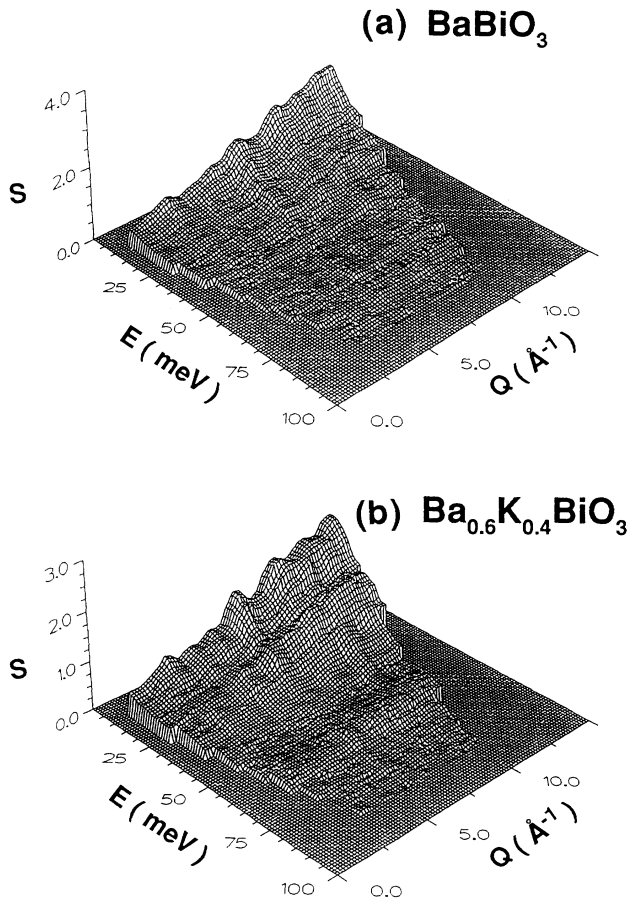

FIG. 3. Experimental inelastic-neutron-scattering dynamic structure factor, $S(Q,E)$, for ^{16}O samples of (a) insulating $Ba_{0.6}K_{0.4}BiO_3$ and (b) superconducting $Ba_{0.6}K_{0.4}BiO_3$ measured by LRMECS with $E_0=120$ meV at 15 K.

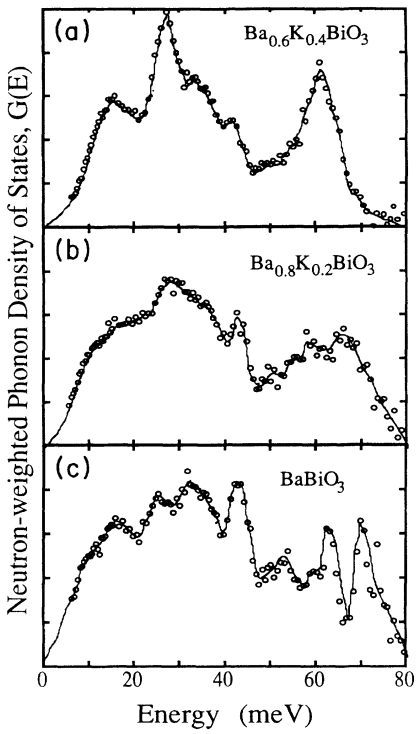

FIG. 4. Experimental neutron-weighted generalized phonon DOS, $G(E)$, for ^{16}O samples of (a) superconducting $Ba_{0.6}K_{0.4}BiO_3$, (b) insulating $Ba_{0.8}K_{0.2}BiO_3$, and (c) parent material $BaBiO_3$ measured by HRMECS with $E_0=110$ meV at 15 K.

upon oxygen isotope substitution. The measured phonon DOS from INS will be discussed in Sec. V along with the results of MD simulations.

IV. MOLECULAR-DYNAMICS SIMULATIONS OF PHONON DENSITY OF STATES

Partial and total phonon densities of states for $BaBiO_3$ and $Ba_{0.6}K_{0.4}BiO_3$ were calculated using the molecular-dynamics method.[33] The MD simulations on $BaBiO_3$ were performed on a 540-particle system in the orthorhombic phase ($a=6.2000$ Å, $b=6.1561$ Å, $c=8.6948$ Å) at the experimental density of 7.88 g/cm^3. The $Ba_{0.6}K_{0.4}BiO_3$ system was obtained by randomly replacing 40% of the Ba atoms with K atoms in a 625-particle system at the experimental density of 7.33 g/cm^3 in the cubic phase ($a=4.3160$ Å). Effective interparticle interactions were used in the MD simulations. The long-range nature of the Coulomb interaction is taken into account by Ewald's summation method.[33] The Newtonian equations of motion are integrated by Beeman's method[34] using a time step of $\Delta t=5\times10^{-15}$ sec, which conserves energy to better than 1 part in 10^4 over several thousand time steps. To explore the effects arising from changes in the symmetry between the cubic and orthorhombic structures, we also simulate a cubic $BaBiO_3$ system. Simulations for isotopically substituted orthorhombic $BaBi(^{18}O)_3$ and cubic $Ba_{0.6}K_{0.4}Bi(^{18}O)_3$ were performed by replacing the ^{16}O mass with that of ^{18}O.

A. Effective interaction potentials

Effective pairwise interactions were used in the MD simulations. The potentials[35] include Coulomb interactions due to charge-transfer effects, charge-dipole interactions due to large electronic polarizability of O^{2-} ions, and steric repulsion between ions. The total interparticle interaction has the form

$$V_{ij}(r)=\frac{Z_iZ_j}{r}-\frac{(\alpha_iZ_j^2+\alpha_jZ_i^2)}{2r^4}\exp\left[-\frac{r}{r_{4s}}\right]+\frac{H_{ij}}{r^{\eta_{ij}}}\ , \tag{5}$$

where Z_i and α_i are the effective charge and electronic polarizability, respectively, of the ith ion and H_{ij} and η_{ij} are, respectively, the strengths and exponents of the steric repulsion between the ions i and j. The screening length, r_{4s}, is chosen so that charge-dipole interaction does not have a long tail. The steric repulsion balances the attractive interactions between cations and anions at short distances so as to give the correct bond lengths. There are six interaction potentials for $BaBiO_3$ and ten

TABLE I. Constants in the effective potentials, Eq. (5), for $BaBiO_3$. The unit of length is Å and that of energy $e^2/Å = 14.39$ eV. Z is the effective charge (in units of $|e|$), α the electronic polarizability (Å^3), η the repulsive exponents, and H the repulsive strengths.

	Z	α
Ba	0.800	0.00
Bi	1.600	0.00
O	−0.800	2.40
r_{4s}	4.430	
	η	H
Ba-Ba	11	1186.8
Ba-Bi	11	157.3
Ba-O	9	281.7
Bi-Bi	11	13.2
Bi-O	9	60.8
O-O	7	49.2

for $Ba_{0.6}K_{0.4}BiO_3$. The parameters for the interaction potentials, used in Eq. (5), for $BaBiO_3$ and $Ba_{0.6}K_{0.4}BiO_3$ are summarized in Tables I and II, respectively. The potentials for $BaBiO_3$ and $Ba_{0.6}K_{0.4}BiO_3$ are displayed in Figs. 5 and 6.

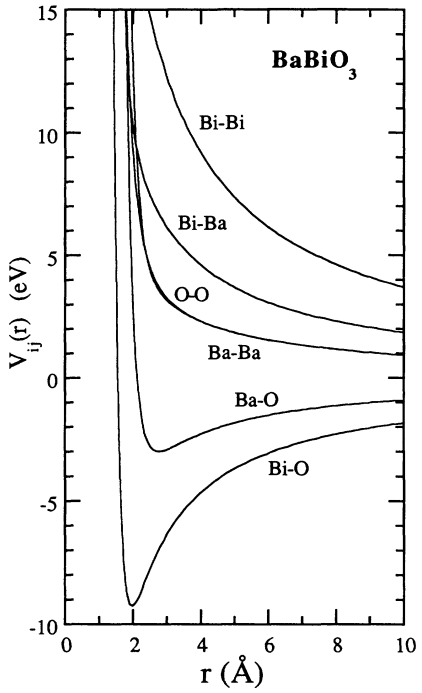

FIG. 5. Six effective interaction potentials for $BaBiO_3$.

B. Dynamical stability

Before calculating the phonon DOS, it was ensured through a procedure shown schematically in Fig. 7 that the systems were dynamically stable in the appropriate symmetries at the correct densities. To establish the dynamical stability of $BaBiO_3$, the system was put in the orthorhombic structure in a MD cell of fixed volume.

TABLE II. Constants in the effective potentials, Eq. (5), for $Ba_{0.6}K_{0.4}BiO_3$. The unit of length is Å and that of energy $e^2/Å = 14.39$ eV. Z is the effective charge (in units of $|e|$), α the electronic polarizability (Å^3), η the repulsive exponents, and H the repulsive strengths.

	Z	α
Ba	0.800	0.00
K	0.400	0.00
Bi	1.600	0.00
O	−0.747	2.40
r_{4s}	4.430	
	η	H
Ba-Ba	11	1007.0
Ba-K	11	1007.0
Ba-Bi	11	133.5
Ba-O	9	239.0
K-K	11	1007.0
K-Bi	11	133.5
K-O	9	239.0
Bi-Bi	11	11.2
Bi-O	9	51.6
O-O	7	41.8

The partial pair distribution functions and bond-angle distribution functions were calculated. The system was then slowly heated to 600 K and thermalized for 30 000 time steps. After this it was run uninterruptedly for more than 30 000 time steps and various structural correlations were calculated to examine the symmetry. The system was then cooled slowly, thermalized, and then subjected to a steepest-descent quench[36] (SDQ) which is a mathematically well-defined method of examining the underlying mechanically stable structures.[37] The partial pair correlation functions and bond-angle distribution functions were calculated again to ascertain the symmetry of the MD system. After performing the above-mentioned procedure on the 540-particle $BaBiO_3$ system, we found the resulting final symmetry to be the same as that of the starting orthorhombic structure. The 625-particle cubic $Ba_{0.6}K_{0.4}BiO_3$ system was also subjected to the same procedure to ensure dynamic stability.

C. Calculation of phonon density of states

Phonon densities of states are calculated using three different methods.[38–41] The first method involves calculating the velocity autocorrelation function for each species and the partial phonon DOS $F_i(\omega)$ is obtained by the Fourier transforms of this autocorrelation functions. The second method involves the displacement autocorrelation functions calculated by the equation-of-motion method. The third method is simply a direct diagonalization of the dynamical matrix. We find that the results of all these three calculations are in agreement with one another.[41] Each of these methods will be described below. Throughout the paper, E and ω are used for energy interchangeably.

1. *Velocity autocorrelation function*

The normalized velocity-velocity autocorrelation function for the βth species (β=Ba, Bi, K, or O) is given by

$$\Gamma_\beta(t)=\frac{\left\langle \sum_{i_\beta=1}^{N_\beta} \mathbf{v}_{i_\beta}(t)\cdot\mathbf{v}_{i_\beta}(0)\right\rangle}{\left\langle \sum_{i_\beta=1}^{N_\beta} \mathbf{v}_{i_\beta}(0)\cdot\mathbf{v}_{i_\beta}(0)\right\rangle} \quad \text{with } \beta\in\{\text{Ba,Bi,K,O}\} , \tag{6}$$

where $\mathbf{v}_{i_\beta}$ is the velocity of particle i_β and $\langle \cdots \rangle$ is an average over MD configurations. At low temperatures,[38] the frequency spectrum of the normalized velocity autocorrelation function gives the partial phonon density of states

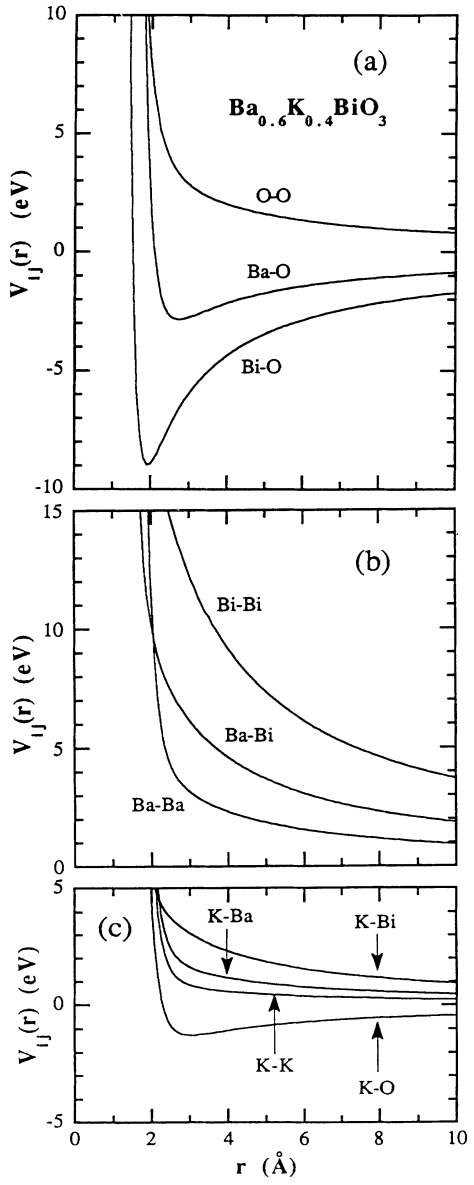

FIG. 6. Ten effective interaction potentials for $Ba_{0.6}K_{0.4}BiO_3$.

$$F_\beta(\omega)=\int_0^\tau \Gamma_\beta(t)\cos(\omega t)e^{-\gamma(t/\tau)^2}dt , \tag{7}$$

where a Gaussian window function with $\gamma=1$ and $\tau=3$ ps is used. The total phonon DOS is obtained by summing over the partial DOS weighted with the concentration

$$F(\omega)=\sum_\beta c_\beta F_\beta(\omega) , \tag{8}$$

where c_β is the concentration of the βth species in the MD system. The neutron-weighted phonon DOS, $G(\omega)$, can be calculated from $F_\beta(\omega)$ using Eq. (4).

2. *Displacement autocorrelation function and equation-of-motion method*

The second method to calculate the phonon DOS involves the displacement autocorrelation function and the equation-of-motion method.[39,40] To implement this scheme, it is essential to bring the system to a local minimum energy state where the force and the velocity of each particle is zero. This was done by carrying out a steepest descent quench on a MD configuration and determining the resulting equilibrium positions $r_{i\mu}(0)$ ($\mu=x,y,z$) of all the particles ($i=1,2,\ldots,N$). Each particle is then given a random displacement

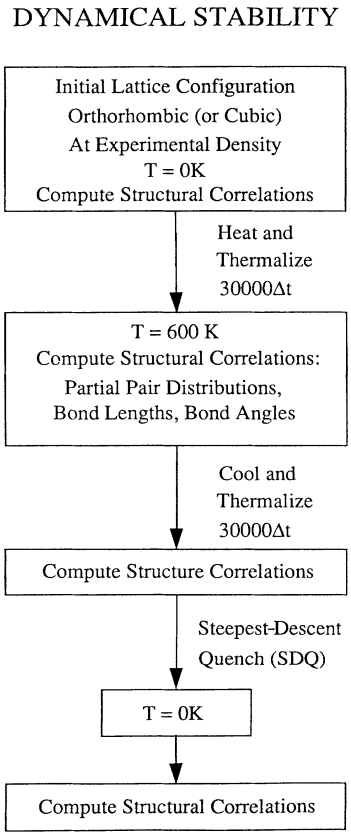

FIG. 7. Schematic diagram showing the procedure to establish dynamical study for a MD system before calculating the phonon density of states.

$$\delta_{i\mu}(0)=\delta_0\cos(\theta_{i\mu}) , \tag{9}$$

where δ_0 is the amplitude of an initial displacement and $\theta_{i\mu}$ are random variables distributed uniformly between 0 and 2π. The system is allowed to evolve according to the classical equations of motion and the time variation of $r_{i\mu}(t)$ obtained. The displacement autocorrelation function is given by

$$f(t)=\sum_{i,\mu}\delta r_{i\mu}(t)\delta r_{i\mu}(0) , \tag{10}$$

where

$$\delta r_{i\mu}(t)=r_{i\mu}(t)-r_{i\mu}(0) . \tag{11}$$

In the harmonic limit,[39] the frequency spectrum of $f(t)$ gives the density of states

$$F(\omega)=\frac{4}{\pi\delta_0^2}\int_0^{\tau}f(t)\cos(\omega t)e^{-\gamma(t/\tau)^2}dt , \tag{12}$$

where a Gaussian window function is used.

3. *Dynamical matrix*

In this method, we first apply the steepest descent quench to a low-temperature MD configuration to bring the system to a minimum energy state. Since the system is dynamically stable, we can calculate the elements of the dynamical matrix **D** from the second derivatives of the potential with respect the x, y, and z coordinates of each particle, i.e.,

$$D_{ij}^{\mu\nu}=-(m_i m_j)^{-1/2}\frac{\partial^2 V}{\partial r_{i\mu}\partial r_{j\nu}} , \tag{13}$$

where m_i is the mass of the ith particle and V is the total potential energy of the system. **D** is a $3N\times 3N$ matrix. The eigenvalues and eigenvectors of the dynamic matrix satisfy the following $3N$ equations of motion:

$$\sum_{j=1}^{N}\sum_{\nu=1}^{3}(D_{ij}^{\mu\nu}-\omega^2\delta_{ij}\delta_{\mu\nu})u_{j\nu}=0 . \tag{14}$$

The matrix elements are calculated numerically for the 540-particle $BaBiO_3$ and the 625-particle $Ba_{0.6}K_{0.4}BiO_3$ systems. We have diagonalized a 1620×1620 dynamical matrix for $BaBiO_3$ and a 1875×1875 matrix for $Ba_{0.6}K_{0.4}BiO_3$ to obtain the eigenvectors and eigenvalues, from which the partial and total density of states are calculated.

V. RESULTS AND DISCUSSION

To identify the physical origin of the peaks in the total DOS, we first examine the MD partial DOS for the insulating $BaBiO_3$ and superconducting $Ba_{0.6}K_{0.4}BiO_3$. Figure 8 displays the MD partial DOS, $F_{Ba}(\omega)$, $F_{Bi}(\omega)$, and $F_O(\omega)$, and also the total DOS $F(\omega)$ for $BaBi(^{16}O)_3$. The partial-phonon DOS, $F_i(\omega)$, is normalized to $3N_i$ such that $\int F_i(\omega)d\omega=3N_i$, where N_i is the total particle number for the ith species in the MD system. It can be seen that there is a clear delineation in the peaks associated with Ba and Bi on the one hand and O on the other. $F_{Ba}(\omega)$ exhibits a single peak at 11 meV, $F_{Bi}(\omega)$ shows two peaks at 12 and 17 meV, and all the peaks in $F_O(\omega)$ are located between 20 and 80 meV. Clearly, in the total DOS [Fig. 8(d)], the peak at 11 meV is due to both Ba and Bi and the peak at 16 meV is due to Bi alone. Above 20 meV the entire spectrum arises from oxygen vibrations. To determine the phonon modes that are likely to be affected by the cubic-to-orthorhombic transformation in $BaBi(^{16}O)_3$, we compare the MD total phonon DOS for cubic and orthorhombic $BaBi(^{16}O)_3$. As Fig. 9 shows, the positions of the Ba (11 meV), O (36 meV), and O (52 meV) peaks are unchanged whereas other peaks are shifted slightly.

Next we examine the MD partial DOS, $F_{Ba}(\omega)$, $F_K(\omega)$, $F_{Bi}(\omega)$, and $F_O(\omega)$, and the total DOS $F(\omega)$ for superconducting $Ba_{0.6}K_{0.4}Bi(^{16}O)_3$. These results, shown in Fig. 10, reveal that the peaks above 20 meV are due to oxygen vibrations. In contrast to $BaBi(^{16}O)_3$, $F_K(\omega)$ for $Ba_{0.6}K_{0.4}Bi(^{16}O)_3$ shows an additional peak at 20 meV

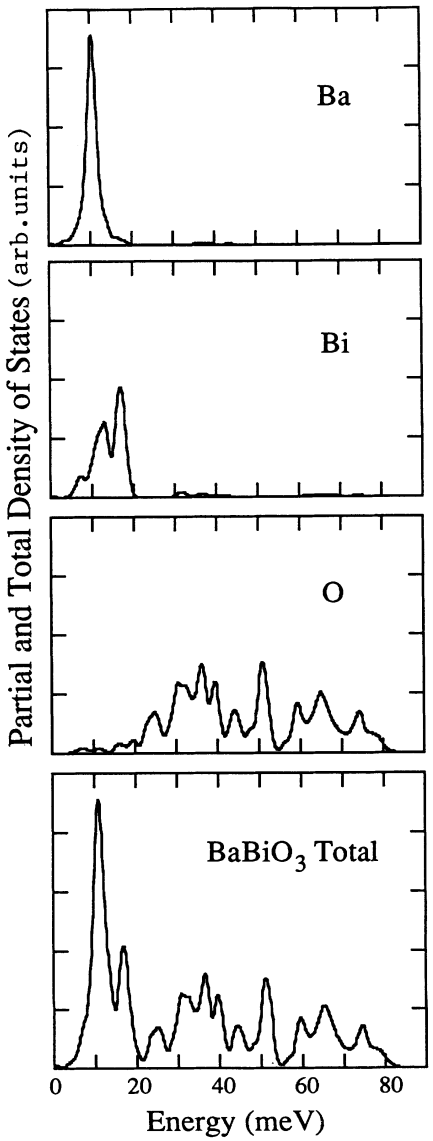

FIG. 8. Molecular-dynamics results of partial and total phonon DOS for orthorhombic $BaBi(^{16}O)_3$.

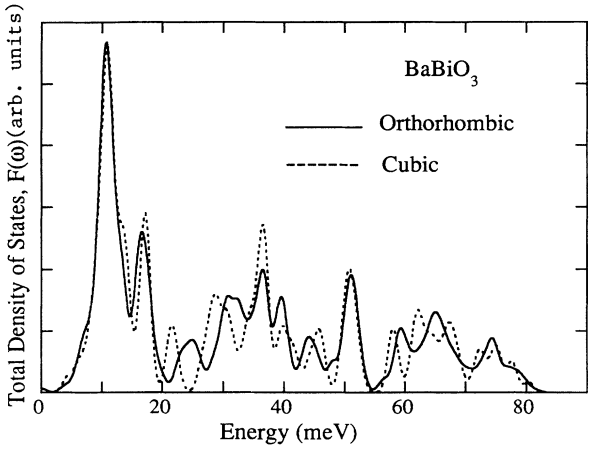

FIG. 9. Molecular-dynamics results of total phonon DOS for orthorhombic and cubic $BaBi(^{16}O)_3$ at the same density.

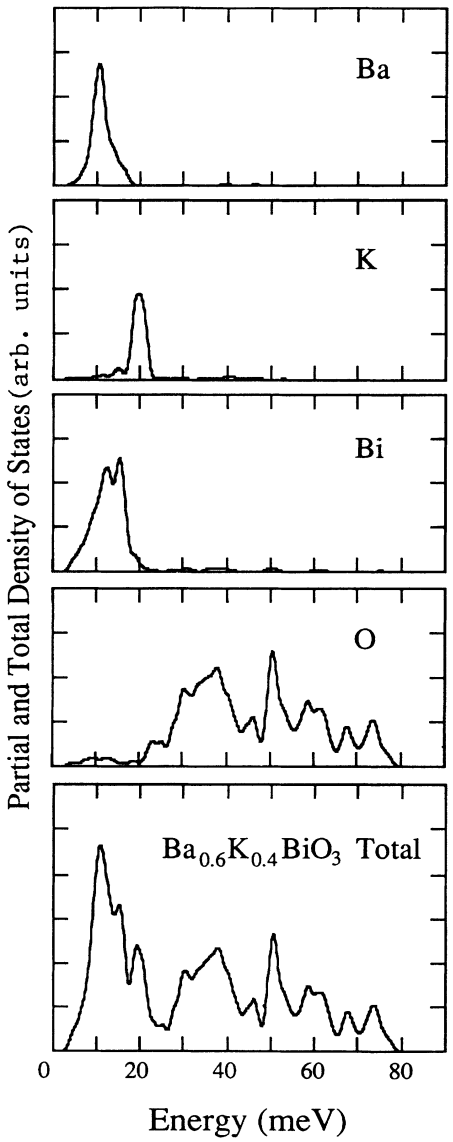

FIG. 10. Molecular-dynamics results of partial and total phonon DOS for cubic $Ba_{0.6}K_{0.4}Bi(^{16}O)_3$.

and the two-peak feature in $F_{Bi}(\omega)$ is less pronounced. The total phonon spectrum, $F(\omega)$, is broadened around 15 meV. There are also significant differences in the oxygen DOS between $BaBi(^{16}O)_3$ and $Ba_{0.6}K_{0.4}Bi(^{16}O)_3$. $F_O(\omega)$ of $BaBiO_3$ clearly shows sharp peaks around 26, 32, 37, 40, 44, 51, 60, 66, and 74 meV. In $Ba_{0.6}K_{0.4}BiO_3$ the peaks between 20 and 40 meV merge into a band, and those between 60 and 80 meV broaden and show a slight shift to lower energies. As a result, the total DOS of $Ba_{0.6}K_{0.4}BiO_3$ above 20 meV not only exhibits broader peaks but also terminates at a lower energy.

We now consider the isotope effect of ^{16}O and ^{18}O substitution on the phonon DOS of $BaBiO_3$. The MD total DOS for the ^{16}O and ^{18}O compounds are shown in Fig. 11. We find a 4–5-meV shift toward lower energies for the phonons of $BaBi(^{18}O)_3$ in the energy region 20–80 meV. As expected, the DOS for both materials are identical at energies below 20 meV where there is no contribution from oxygen vibrations. This is also true for the DOS of $Ba_{0.6}K_{0.4}Bi(^{18}O)_3$, as shown in Fig. 12.

We now discuss the comparison of MD results with the INS data. In order to compare the neutron data with MD simulation, we have calculated the neutron-weighted DOS, $G(\omega)$, using the MD partial DOS in Eq. (4). The results are shown in Figs. 13 and 14 for $BaBiO_3$ and $Ba_{0.6}K_{0.4}BiO_3$, respectively. In general, there is an overall qualitative agreement between the MD results and neutron spectra. In the case of $BaBiO_3$, the low-energy peaks at 11 and 17 meV cannot be resolved in the neutron data due to the relatively poor resolution in this energy region. The difference between the MD and neutron $G(\omega)$ in the relative magnitude of the low-energy DOS is probably due to resolution effects and uncertainties of multiple-scattering background in the INS experiments. Otherwise, the peaks at 25, 30–40, 50, 60, and 65–75 of the MD DOS are identifiable with similar structures in the measured DOS. For $Ba_{0.6}K_{0.4}BiO_3$, the MD $G(\omega)$ shows a three-band structure with intensities centered around 14, 35, and 65 meV. Although the energies are slightly higher (by ~ 5 meV) in the MD results than the observed values, these phonon bands resemble closely

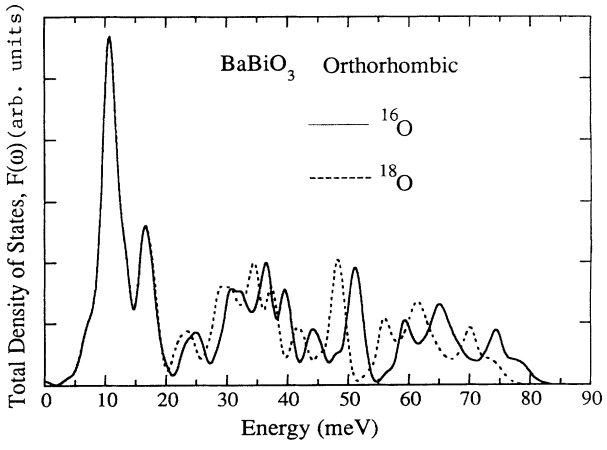

FIG. 11. Molecular-dynamics results of total phonon DOS for orthorhombic $BaBi(^{16}O)_3$ and orthorhombic $BaBi(^{18}O)_3$.

the neutron data. Furthermore, symmetry analysis of the phonon modes around 33 and 60 meV reveals that they are mainly due to symmetric breathing motion of the oxygen atoms around Bi and K (or Ba) atoms. The major discrepancy between the experimental and simulation results for both $BaBiO_3$ and $Ba_{0.6}K_{0.4}BiO_3$ is that the MD spectra show a peak around 50 meV whose amplitude in the experimental $G(\omega)$ is considerably smaller. Although the MD simulations were carried out with effective pair potentials which include steric repulsions, Coulomb interactions, and electronic polarization effects of the ions, microscopic interactions between electrons and phonons were not incorporated explicitly. Therefore, it is perhaps not surprising to find the discrepancy between the measured and calculated phonon DOS. Nevertheless, the calculations yield the phonon spectra for both $BaBiO_3$ and

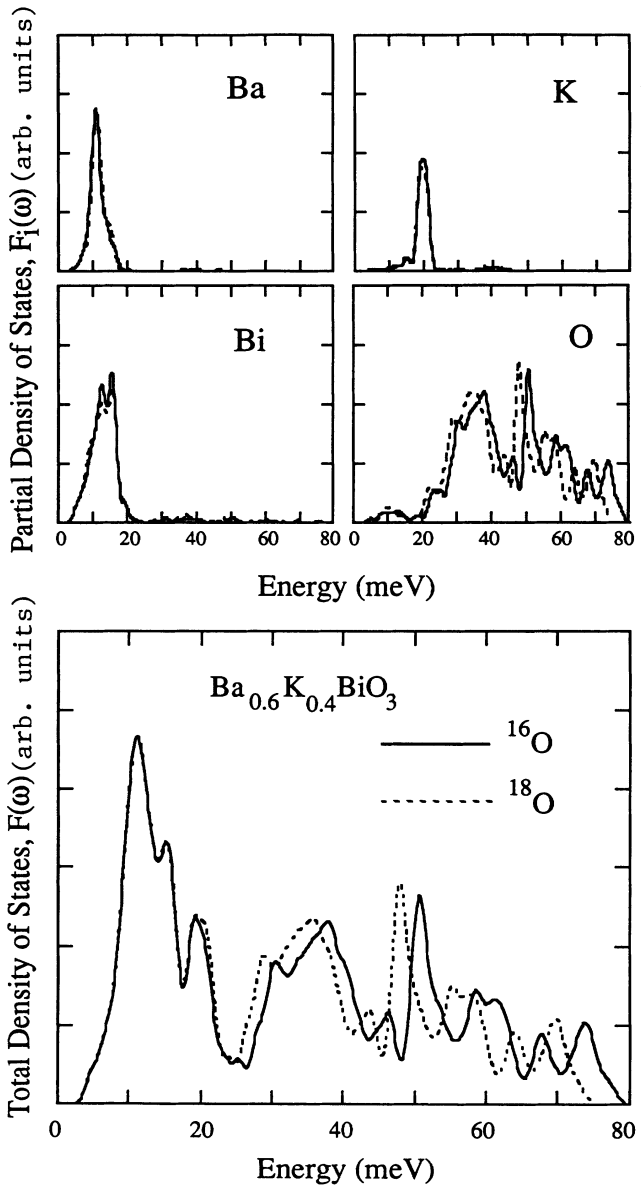

FIG. 12. Molecular-dynamics results of partial and total phonon DOS for cubic $Ba_{0.6}K_{0.4}Bi(^{16}O)_3$ and cubic $Ba_{0.6}K_{0.4}Bi(^{18}O)_3$.

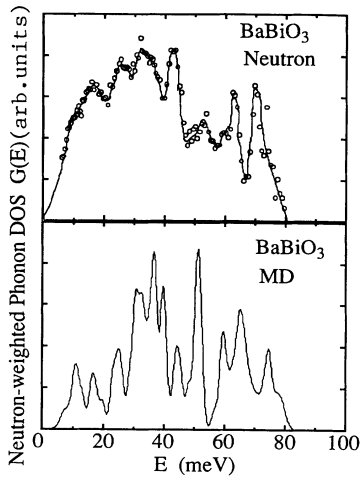

FIG. 13. Neutron-weighted phonon DOS for $BaBi(^{16}O)_3$. Upper panel: INS experimental values (the solid line is a guide to the eye); lower panel: molecular-dynamics results.

$Ba_{0.6}K_{0.4}BiO_3$ on a correct energy scale and confirm the origin of mode broadening and softening in $Ba_{0.6}K_{0.4}BiO_3$.

It is clear from INS measurements and MD simulation that the oxygen phonon modes soften by 5–10 meV with 40% K doping of $BaBiO_3$. The softening occurs for the following reason: With the substitution of Ba by K, it has been found[42] experimentally that there are holes on the oxygen $2p$ orbitals which screen the charge on the oxygen anions. Since the scale of energy is determined by the charge on oxygen, a reduction due to screening lowers the energy of these modes. Furthermore, INS experiments and MD simulation also suggest that the strongest phonon features in superconducting $Ba_{0.6}K_{0.4}BiO_3$ occur around 30 and 60 meV. In recent tunneling experiments, strong features at these energies in the second derivative of the tunneling current and in

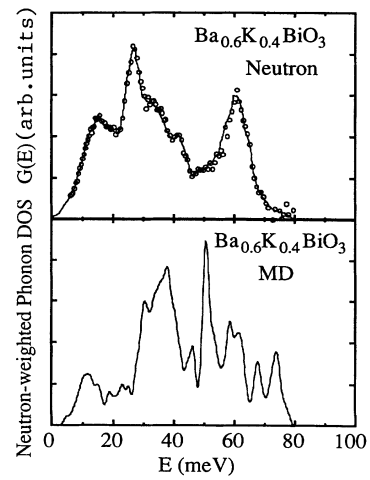

FIG. 14. Neutron-weighted phonon DOS for $Ba_{0.6}K_{0.4}Bi(^{16}O)_3$. Upper panel: INS experimental values (the solid line is a guide to the eye); lower panel: molecular-dynamics simulation results.

the inverted $\alpha^2F(\omega)$ are also observed.[17,18] Thus, the cumulative evidence from the MD simulations and neutron and tunneling measurements suggests that the coupling of electrons to 30- and 60-meV oxygen phonons is responsible for superconductivity in $Ba_{0.6}K_{0.4}BiO_3$.

In a recent calculation of electron-phonon interactions in $Ba_{1-x}K_xBiO_3$ based on a tight-binding approach, Shirai *et al.*[43] find that electron-lattice coupling causes significant energy reduction and line broadening of the longitudinal phonons involving oxygen stretching and/or breathing vibrations around 60 meV. These results are in good agreement with our neutron data and MD simulation. In principle, neutron spectroscopy can also be applied to investigate the phonon dispersion relations and lifetime effects in $Ba_{1-x}K_xBiO_3$, such as the studies[44] of phonons in the copper-oxide superconductors. However, to the best of our knowledge, similar measurements have not been done on $Ba_{1-x}K_xBiO_3$ due to the unavailability of large, good-quality single crystals of these materials.

VI. ISOTOPE EFFECT IN PHONON DENSITY OF STATES AND SUPERCONDUCTING TRANSITION TEMPERATURE

For a BCS superconductor,[25] isotopic substitution of a particular atomic species will effect the superconducting transition temperature as well as the phonon spectrum. The variation of T_c upon oxygen isotopic substitution is characterized by the oxygen-isotope-effect exponent, α_O:

$$\alpha_O = -\frac{\partial \ln T_c}{\partial \ln M_O} , \tag{15}$$

where M_O is the mass of the oxygen isotope. From the strong-coupling theory of superconductivity,[45–48] the result for the transition temperature of a superconductor can always be written as

$$T_c = \langle \omega \rangle e^{-f(\lambda,\ldots,\mu^*)} , \tag{16}$$

where $f(\lambda,\ldots,\mu^*)$ is an unknown functional determined from the solution of the Eliashberg gap equations without any weak-coupling approximation, λ is a dimensionless electron-phonon coupling constant, and μ^* is the Coulomb pseudopotential. The characteristic phonon frequency $\langle \omega \rangle$ is defined as the first frequency moment

$$\langle \omega \rangle = \frac{\int_0^\infty \omega F(\omega) d\omega}{\int_0^\infty F(\omega) d\omega} . \tag{17}$$

The oxygen-isotope-effect exponent in Eq. (15) can be written as a sum of two terms obtained by differentiating Eq. (16):

$$\alpha_O = \alpha_{Or} - \frac{\partial[-f(\lambda,\ldots,\mu^*)]}{\partial \ln M_O} , \tag{18}$$

where α_{Or} is the *reference*-isotope-effect exponent defined by

$$\alpha_{Or} = -\frac{\partial \ln \langle \omega \rangle}{\partial \ln M_O} . \tag{19}$$

Thus, the reference-isotope-effect exponent reflects the mass variation of the phonon DOS in a material whereas the oxygen mass variation of T_c is given by the isotope-effect exponent α_O. Therefore, the deviation of α_O from α_{Or},

$$\delta\alpha_O = \alpha_{Or} - \alpha_O = -\frac{\partial f(\lambda,\ldots,\mu^*)}{\partial \ln M_O} , \tag{20}$$

is a measure of the contribution arising from the factor $\exp[-f(\lambda,\ldots,\mu^*)]$ which contains the strong-coupling effects.

For monatomic BCS superconductors, $\alpha_r = \alpha = \frac{1}{2}$. In the presence of strong-coupling effects, α will deviate from α_r due to a significant contribution from the factor $\exp[-f(\lambda,\ldots,\mu^*)]$. For multicomponent systems such as $Ba_{1-x}K_xBiO_3$, a *partial* isotope-effect exponent α_{ri} or α_i, may be quite different[47] from $\frac{1}{2}$ for isotopic substitution of the ith atomic species, e.g., ^{18}O for ^{16}O. Thus, a measurement of α_O alone does not provide enough information to assess the importance of strong-coupling effects. A large $\delta\alpha_i$, on the other hand, implies that the strong-coupling effects are important. Therefore, the assessment of strong-coupling effects in a superconductor with many atomic species requires the knowledge of the reference-isotope-effect exponent α_{Or}.

Figure 15 shows the neutron-weighted phonon DOS, $G(E)$, for the ^{16}O and ^{18}O samples of $Ba_{0.6}K_{0.4}BiO_3$ obtained from INS and from MD simulations. The MD $G(E)$ in Fig. 15 has been convolved with the experimental resolution function.[49] The overall shape of the phonon DOS for the ^{18}O sample is similar to that for the ^{16}O sample, except that above 20 meV the phonon spectrum is shifted to lower energies by 3–4 meV. The experimental $G(E)$ displays three major phonon bands around 15,

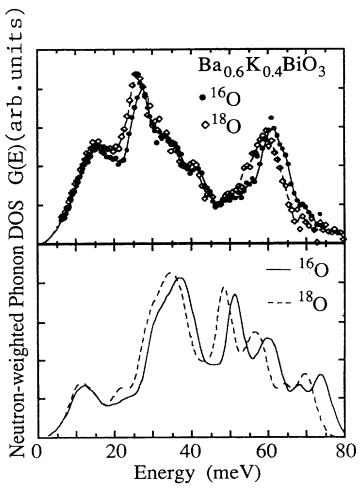

FIG. 15. Neutron-weighted phonon DOS for $Ba_{0.6}K_{0.4}Bi(^{16}O)_3$ and $Ba_{0.6}K_{0.4}Bi(^{18}O)_3$. Upper panel: INS experimental values (the solid lines are guides to the eye); lower panel: molecular-dynamics results, convolved with the experimental resolution function.

30, and 60 meV. The corresponding features above 20 meV in the MD results have slightly higher energies. The experimental estimate of the energy shift between the ^{16}O and ^{18}O phonon DOS, after accounting for the 74% ^{18}O in the isotopically substituted sample, agrees well with the value calculated from the MD results. As it was pointed out earlier in Sec. V, the overall agreement between the INS and MD results for $G(E)$ is good. From the neutron results for $G(E)$, we calculate a neutron-weighted moment $\langle\bar{\omega}\rangle=\int dE\, EG(E)/\int dE\, G(E)$. The mass variation of $\langle\bar{\omega}\rangle$ gives a neutron-weighted reference-isotope-effect exponent 0.49 after correcting for the 74% isotopic substitution in the ^{18}O sample. Using the MD results for $G(\omega)$, we find a neutron-weighted exponent of 0.48, in excellent agreement with the experimental value. This confirms the reliability of the MD DOS.

Having established that the MD results for $G(\omega)$ and its first moment are in accord with the neutron-scattering measurements, we can use the total phonon DOS, $F(\omega)$, from the MD simulation to calculate the exponent α_{Or}. The reference-isotope-effect exponent α_{Or} is found to be 0.42, which is only slightly larger than the experimental values of α_O measured by Hinks *et al.*[14] (0.41±0.03) and by Kondoh *et al.*[11] (0.35±0.05) from T_c, but significantly different from the results of Batlogg *et al.*[5] (0.22±0.03). From Eq. (20) we derive $\delta\alpha_O=0.1\pm0.06$, indicating that $Ba_{1-x}K_xBiO_3$ is a weak-to moderate-coupling superconductor.

VII. CONCLUSION

In conclusion, this paper describes INS measurements and MD simulations of isotopically substituted samples of an oxide superconductor. The comparison of the phonon DOS of the superconducting $Ba_{0.6}K_{0.4}BiO_3$ with those of the parent nonsuperconducting materials provides evidence for the importance of electron-phonon interaction in the superconducting $Ba_{1-x}K_xBiO_3$. By combining the INS and MD results, the reference-isotope-effect exponent of oxygen, α_{Or}, is estimated to be 0.42, only slightly higher than the isotope-effect exponent for T_c, $\alpha_O=0.41$. This result suggests that $Ba_{1-x}K_xBiO_3$ is a weak- to moderate-coupling BCS-like superconductor. The high-T_c results from large electron-phonon matrix elements involving high-energy oxygen phonons.[50]

ACKNOWLEDGMENTS

The work is supported in part by a grant from Louisiana Education Quality Support Fund under Grant No. LEQSF-(1991-92)-RD-A-05. M. H. D. would like to thank Fundacão de Amparo a Pesquisa do Estado de São Paulo (FAPESP), Brazil for partial support. B. D., D. R. R., and Y. Z. were supported by the NSF Technology Center for Superconductivity (under Grant No. DMR88-09854). This work is supported in part by the U.S. Department of Energy, Basic Energy Sciences-Materials Sciences, under Contract No. W-31-109-ENG-38.

*Permanent address: Instituto de Física e Química de São Carlos-USP, São Carlos, Brazil.

[1] J. C. Phillips, *Physics of High-T_c Superconductors* (Academic, San Diego, 1989); *High Temperature Superconductivity-The Los Alamos Symposium,* edited by K. S. Bedell, D. Coffey, D. E. Meltzer, D. Pines, and J. R. Schrieffer (Addison-Wesley, California, 1990).

[2] I. K. Schuller and J. D. Jorgensen, Mater. Res. Bull. **14**, 27 (1989); J. D. Jorgensen and D. G. Hinks, Neutron News **1**, 24 (1991).

[3] L. F. Mattheiss, E. M. Gyorgy, and D. W. Johnson, Jr., Phys. Rev. B **37**, 3745 (1988).

[4] R. J. Cava, B. Batlogg, J. J. Krajewski, R. Farrow, L. W. Rupp, Jr., A. E. White, K. Short, W. F. Peck, and T. Kometani, Nature **332**, 814 (1988).

[5] B. Batlogg, R. J. Cava, L. W. Rupp, Jr., A. M. Mujsce, J. J. Krajewski, J. P. Remeika, W. F. Peck, Jr., A. S. Cooper, and G. P. Espinosa, Phys. Rev. Lett. **61**, 1670 (1988).

[6] D. G. Hinks, B. Dabrowski, J. D. Jorgensen, A. W. Mitchell, D. R. Richards, S. Pei, and D. Shi, Nature **333**, 836 (1988).

[7] D. G. Hinks, D. R. Richards, B. Dabrowski, A. W. Mitchell, J. D. Jorgensen, and D. T. Marx, Physica C **156**, 477 (1988).

[8] D. G. Hinks, A. W. Mitchell, Y. Zheng, D. R. Richards, and B. Dabrowski, Appl. Phys. Lett. **54**, 1585 (1989).

[9] S. Pei, J. D. Jorgensen, B. Dabrowski, D. G. Hinks, D. R. Richards, A. W. Mitchell, J. M. Newsam, S. K. Sinha, D. Vaknin, and A. J. Jacobson, Phys. Rev. B **41**, 4126 (1990).

[10] Y. J. Uemura, B. J. Sternlieb, D. E. Cox, J. H. Brewer, R. Kadono, J. R. Kempton, R. F. Kiefl, S. R. Kreitzman, G. M. Luke, P. Mulhern, T. Riseman, D. L. Williams, W. J. Kossler, X. H. Yu, C. E. Stronach, M. A. Subramanian, J. Gopalakrishnan, and A. W. Sleight, Nature **335**, 151 (1988).

[11] S. Kondoh, M. Sera, Y. Ando, and M. Sato, Physica C **157**, 469 (1989).

[12] B. Batlogg, R. J. Cava, L. F. Schneemeyer, and G. P. Espinosa, IBM J. Res. Develop. **33**, 208 (1989); B. Batlogg, in *Mechanisms of High Temperature Superconductivity,* edited by H. Kamimura and A. Oshiyama (Springer-Verlag, Berlin, 1989), p. 324.

[13] M. Weger and I. B. Goldberg, in *Solid State Physics,* edited by H. Ehrenreich, F. Seitz, and D. Turnbull (Academic, New York, 1973), Vol. 28, p. 1; L. R. Testardi, Rev. Mod. Phys. **47**, 637 (1975); C. C. Yu and P. W. Anderson, Phys. Rev. B **29**, 6165 (1984).

[14] D. G. Hinks, D. R. Richards, B. Dabrowski, D. T. Marx and A. W. Mitchell, Nature **335**, 419 (1988).

[15] S. Hoen, W. N. Creager, L. C. Bourne, M. F. Crommie, T. W. Barbee, III, M. L. Cohen, A. Zettle, L. Bernardez, and J. Kinney, Phys. Rev. B **39**, 2269 (1989).

[16] M. K. Crawford, M. N. Kunchur, W. E. Farneth, E. M. McCarron, III, and S. J. Poon, Phys. Rev. B **41**, 282 (1990); M. K. Crawford, W. E. Farneth, E. M. McCarron, III, R. L. Harlow, and A. H. Moudden, Science, **250**, 1390 (1990); J. P. Franck, J. Jung, M. A. K. Mohamed, S. Gygax, and G. I. Sproule, Physica B **169**, 697 (1991).

[17] J. F. Zasadzinski, N. Tralshawala, D. G. Hinks, B. Dabrowski, A. W. Mitchell, and D. R. Richards, Physica C **158**, 519 (1989); J. F. Zasadzinski, N. Tralshawala, J. Timpf, D. G. Hinks, B. Dabrowski, A. W. Mitchell, and D. R. Richards, Physica C **162-164**, 1053 (1989).

[18]H. Sato, H. Takagi, and S. Uchida, Physica C **169**, 391 (1990).
[19]Z. Schlesinger, R. T. Collins, J. A. Calise, D. G. Hinks, A. W. Mitchell, Y. Zheng, B. Dabrowski, N. E. Bickers, and D. J. Scalapino, Phys. Rev. B **40**, 6862 (1989).
[20]Q. Huang, J. F. Zasadzinski, N. Tralshawala, K. E. Gray, D. G. Hinks, J. L. Peng, and R. L. Greene, Nature **347**, 369 (1990).
[21]C. M. Varma, Phys. Rev. Lett. **61**, 2713 (1988), in *High Temperature Superconductors,* edited by T. Akachi, J. A. Cogordan, and A. A. Valladares (World Scientific, Singapore, 1989), p. 35; E. Jurczek and T. M. Rice, Europhys. Lett. **1**, 255 (1986).
[22]S. Pei N. J. Zaluzec, J. D. Jorgensen, B. Dabrowski, D. G. Hinks, A. W. Mitchell, and D. R. Richards, Phys. Rev. B **39**, 811 (1989); E. A. Hewat, C. Chaillout, M. Godinho, M. F. Gorius, and M. Marezio, Physica C **157**, 228 (1989); M. Verwerft, G. Van Tendeloo, G. D. G. Hinks, B. Dabrowski, D. R. Richards, A. W. Mitchell, G. T. Marx, Shiyou Pei, and J. D. Jorgensen, Phys. Rev. B **44**, 9547 (1991).
[23]P. B. Allen, Nature **339**, 428 (1989).
[24]D. G. Hinks, Mater. Res. **15**, No. 6, 55 (1990).
[25]J. R. Schrieffer, *Theory of Superconductivity* (Benjamin, New York, 1964).
[26]D. J. Scalapino, in *Superconductivity,* edited by R. D. Parks (Dekker, New York, 1969), Vol. 1, p. 449.
[27]Among the measured α_O values, we consider the α_O given by Hinks *et al.* (Ref. 14) more reliable than other values because Hinks *et al.* (Ref. 14) demonstrated the quality of their measurements by reexchanging the sample with ^{16}O, and they chose the composition of the sample to minimize systematic errors (that would lower the measured value of α_O) resulting from the loss of small amounts of potassium during processing.
[28]C.-K. Loong, P. Vashishta, R. K. Kalia, M. H. Degani, D. L. Price, J. D. Jorgensen, D. G. Hinks, B. Dabrowski, A. W. Mitchell, D. R. Richards, and Y. Zheng, Phys. Rev. Lett. **62**, 2628 (1989).
[29]C.-K. Loong, D. G. Hinks, P. Vashishta, W. Jin, R. K. Kalia, M. H. Degani, D. L. Price, J. D. Jorgensen, B. Dabrowski, A. W. Mitchell, D. R. Richards, and Y. Zheng, Phys. Rev. Lett. **66**, 3217 (1991).
[30](a) M. M. Bredov, B. A. Kotov, N. M. Okuneva, V. S. Oskotskii, and Shakh-Budagov, Fiz. Tverd Tela (Leningrad) **9**, 287 (1967) [Sov. Phys. Solid State **9**, 214 (1967)]; (b) V. S. Oskotskii, *ibid.* **9**, 550 (1967) [**9**, 420 (1967)]; (c) E. W. De Wette and A. Rahman, Phys. Rev. **176B**, 784 (1968).
[31]D. L. Price and K. Sköld, in *Neutron Scattering,* edited by K. Sköld and D. L. Price (Academic, Orlando, 1986), Vol. A, Chap. 1, p. 29.
[32]J. M. Carpenter (unpublished).
[33]A. Rahman and P. Vashishta, in *Physics of Superionic Conductors,* edited by J. W. Perram (Plenum, New York, 1983), p. 93.
[34]D. Beeman, J. Comput. Phys. **20**, 130 (1976).
[35]P. Vashista and A. Rahman, Phys. Rev. Lett. **40**, 1337 (1978); P. Vashista, R. K. Kalia, J. P. Rino, and I. Ebbsjö, Phys. Rev. B **41**, 12 197 (1990).
[36]R. Fletcher, *Practical Methods of Optimization* (Wiley, New York, 1980).
[37]B. P. Feuston, R. K. Kalia, and P. Vashishta, Phys. Rev. B **35**, 6222 (1987); **37**, 6297 (1988), G. A. Antonio, B. P. Feuston, R. K. Kalia, and P. Vashishta, J. Chem. Phys. **88**, 7671 (1988).
[38]A. Rahman, M. J. Mandell, and J. P. McTague, J. Chem. Phys. **64**, 1564 (1976).
[39]D. Beeman and R. Alben, Adv. Phys. **26**, 339 (1977).
[40]P. Vashishta, R. K. Kalia, and I. Ebbsjö, Phys. Rev. B **39**, 6034 (1989).
[41]P. Vashishta, M. H. Degani, and R. K. Kalia, in *Correlations in Electronic and Atomic Fluids,* edited by P. Jena, R. K. Kalia, P. Vashishta, and M. P. Tosi (World Scientific, Singapore, 1990), p. 223.
[42]E. Alp (private communication).
[43]Masafumi Shirai, Naoshi Suzuki, and Kazuko Motizuki, J. Phys. Condens. Matter. **2**, 3553 (1990).
[44]L. Pintschovius, Festkörperprobleme **30**, 183 (1990); W. Reichardt, *Neutron News,* **1**, 20 (1990).
[45]W. L. McMillian, Phys. Rev. **167**, 331 (1968).
[46]P. B. Allen and R. C. Dynes, Phys. Rev. B **12**, 905 (1975).
[47]J. P. Carbotte, in *Electron-Phonon Interaction in Oxide Superconductors,* edited by J. P. Carbotte and R. Baquero (World Scientific, Singapore, to be published).
[48]J. P. Carbotte, Rev. Mod. Phys. **62**, 1027 (1990).
[49]C.-K. Loong, S. Ikeda, and J. M. Carpenter, Nucl. Instrum. Methods A **260**, 381 (1987).
[50]C.-K. Loong, D. G. Hinks, W. Jin, M. H. Degani, D. L. Price, J. D. Jorgensen, B. Dabrowski, A. W. Mitchell, D. R. Richards, Y. Zheng, P. Vashista, and R. K. Kalia, in *Electron-Phonon Interaction in Oxide Superconductors,* edited by J. P. Carbotte and R. Baquero (World Scientific, Singapore, to be published).

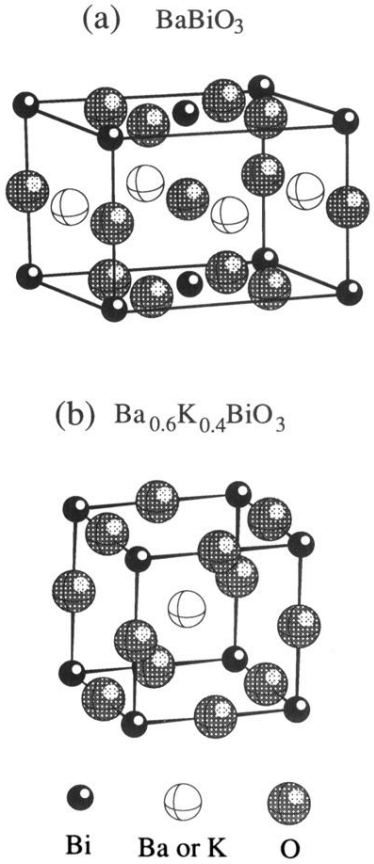

FIG. 1. Crystal structures of (a) orthorhombic $BaBiO_3$ and (b) cubic $Ba_{0.6}K_{0.4}BiO_3$.

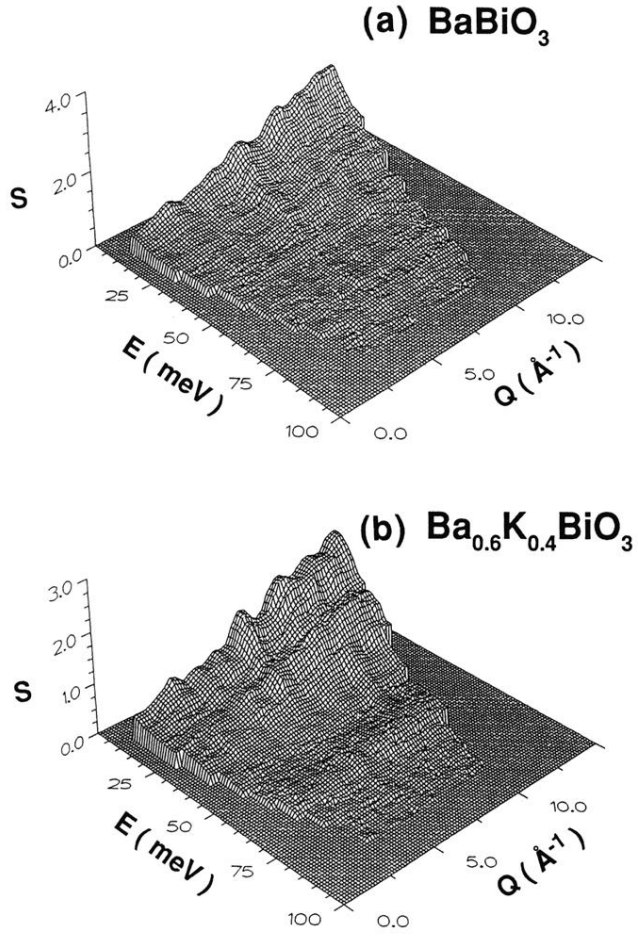

FIG. 3. Experimental inelastic-neutron-scattering dynamic structure factor, $S(Q,E)$, for ^{16}O samples of (a) insulating $Ba_{0.6}K_{0.4}BiO_3$ and (b) superconducting $Ba_{0.6}K_{0.4}BiO_3$ measured by LRMECS with $E_0 = 120$ meV at 15 K.